SHIELDING COSMIC RADIATION IN AIR TRAFFIC

Lily Schrempp*, Andreas Sizmann*
***Bauhaus Luftfahrt e.V., Lyonel-Feininger-Str. 28, 80807 Munich, Germany**
lily.schrempp@bauhaus-luftfahrt.net; andreas.sizmann@bauhaus-luftfahrt.net

Keywords: *Cosmic Radiation Shielding; Liquid Hydrogen; Cryoplane Technology; Nanocomposites*

Abstract

In this study, we confront future trends in air travel concerning polar route frequencies and cruising altitudes with the associated risk arising from cosmic radiation. Furthermore, we identify and evaluate a radiation shielding concept based on both the cryoplane technology as well as on novel nanomaterials. Besides its beneficial impact on the climate, liquid hydrogen as a long-term alternative fuel is shown to allow for substantial co-benefits in radiation shielding, which could open up economic ways for flying beyond and above Earth's natural protection.

1 Introduction

The growing demand of mobility of our society is associated with a continuing increase of air travel. Cross-polar routes directly connecting North America and Asia are subject to an explosive growth and future high-speed commercial air traffic will be flying in ever higher altitudes. In view of these developments, the associated level of exposure of aircrew, frequent flyers and aircraft electronics to cosmic radiation becomes under intense scrutiny and of increasing international concern. In the study at hand, we identify and evaluate a radiation shielding concept, which is based on the so-called cryoplane technology [1, 2, 3], which considers liquid hydrogen as a long-term alternative fuel as a substitute for kerosene [4]. While this technology option is coventionally solely investigated in the context of reducing the climate impact of air traffic, it is our aim to reveal synergy effects, which in combination with recent advances in nano-science, could lead to a substantial reduction in the cosmic radiation exposure of humans in aviation. We discuss in more detail the radiation fields at aircraft altitudes and their impact on humans and equipment in Sec. 1.1, introduce some general aspects about efficient neutron shielding in Sec. 1.2 and finally in Sec. 1.3 further motivate the investigation of the cryoplane technology combined with nanophysics for radiation shielding in aviation.

1.1 Cosmic Radiation Exposure in Air Traffic

The term cosmic radiation collectively comprises highly-energetic primary radiation, mainly protons and Helium nuclei, which originate from the sun as well as from outside of the solar system. It furthermore includes the cascades of secondary cosmic radiation, composed of an electromagnetic component – X-ray and Gamma-radiation – as well as of electrically charged and uncharged subatomic particles, created when the primaries enter the atmosphere and interact with its constituents. The intensity of the various radiation components, which move downwards in the atmosphere, is a function of their energy and depends mainly on altitude. From typical cruising altitudes of long-range airliners to sea level the total particle flux reduces by about a factor of 300 almost linearly with altitude [5]. The reason is that the density of the atmosphere and thus its ability to absorb cosmic particles increases towards the ground, providing some natural radiation protection of the Earth. To a smaller extend, the in-flight exposure grows with latitude,

as the fraction of charged particles shielded by the Earth's magnetic field decreases towards the magnetic poles. The exposure rate at 70 degrees north or south latitude is about four times larger than at 25 degrees such that the total radiation exposure on long-haul cross-polar flights is significantly increased compared to short-haul flights confined to the mid-latitudes. Finally, solar flares can raise the cosmic radiation flux by a factor of 10 to 20 for brief periods of time [6, 7].

The exposure to increased levels of cosmic ionizing radiation in aviation is under scrutiny for two reasons. Firstly, for humans it can lead to chromosome damage and increases the risk of certain types of cancer. Sixty-five epidemiological studies find consistently elevated incidence of breast cancer in female aircrew members and of melanoma in both male and female aircrew [8]. Estimated annual exposure to aircrews equals, if not exceeds, the allowable limits for the average nuclear power plant worker [9]. Frequent-flyer business passengers are more likely to be exposed to even higher doses than the aircrew, because flight hours are not restricted for passengers. For example, five 13-hour cross-polar flights from New York to Tokyo and back, or a single round-trip during a solar storm, already exceed the maximum recommended levels for annual radiation doses for the general public [9]. Secondly, single energetic cosmic particles can cause disturbances to microelectronic components onboard of aircrafts and have become an increasingly important safety issue, since the first reports of in-flight occurrences in the early 1990's. In particular, the continuing trend to smaller, denser, faster and more power-efficient integrated circuits increases the susceptibility. Reduced transistor voltages imply lower thresholds for calculation errors induced by the ionizing field charge from a single energetic particle [10].

The risks associated with radiation exposure in air traffic are expected to further gain significantly in importance in the near future due to the Earth's drifting magnetic poles. In fact, the magnetic north, currently in the Canadian Arctic, roughly 1600 km away from the geographic North Pole, is moving towards Siberia at about 65 km per year [11]. The more it drifts southward and thus towards areas with high air traffic demand, the larger becomes the cosmic radiation exposure in aviation. This is especially problematic in periods, when solar activity and thus the probability for high level solar storms rises as is, for example, currently the case. The occurrence of solar flares in general greatly enhances the operating costs for airlines, since flights are sent to lower altitudes or cross-polar flights have to be rerouted away from the Poles.

While polar routes usually offer direct service, fuel costs and flight times are significantly increased, if the rerouting requires intermediate gas stops. The associated economical penalties are expected to gain in importance, given that the annual number of cross-polar flights has risen from a couple of hundred to almost 10^4 within the last decade and thus on average corresponds to the largest annual growth rate in air traffic within this period [12, 13]. For example, at present, a couple of percent of the Revenue Passenger Kilometers (RPK) of international flights are provided by polar routes, however, the associated average RPK growth rate is with impressive 37% per year roughly 8 times larger than for international flights. This continuing trend mirrors the rapid growth of Asian markets, which drives economic bonding with North America and thus boosts the demand for polar routes in comparison to other segments of air traffic. As a guideline for airline route planning and to enable the assessment of cost and risk of polar routes, scientists at the NASA Langley Research Center currently develop the Nowcast Atmospheric Ionizing Radiation for Aviation Safety (NAIRAS) model with the aim of measuring and monitoring cosmic radiation levels in aviation with real-time immediacy [14].

Concerns regarding the cosmic radiation exposure carry even more authority for future high-speed air traffic at higher altitudes as demonstrated by radiation measurements on board of the supersonic airliner Concorde during its operation time until 2003. In fact the cosmic radiation intensity has a maximum at altitudes varying from roughly 16 to 25 km above sea level [6, 18].

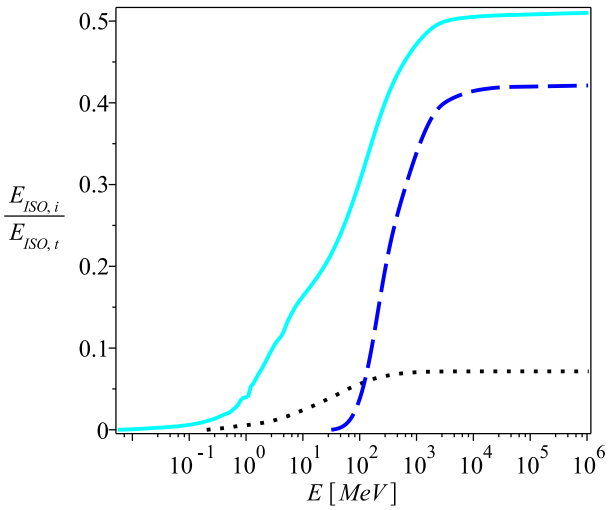

Fig. 1 Fraction of the total effective dose rate respectively provided by neutrons (solid), protons (dashed) and X-rays/Gamma-radiation (dotted) up to an energy E.

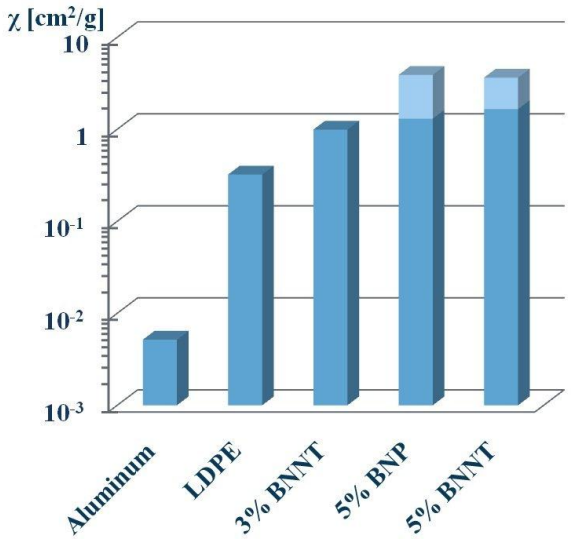

Fig. 2 Mass attenuation coefficient χ as a measure for the effectiveness of neutron shielding in relation to the mass penalty for low-density Polyethylen (LDPE), low loading Boron Nitride Nanoparticle (BNP) and Boron Nitride Nanotube (BNNT)/polymide composites (based on data of Ref. 15) as well as for aluminum as a benchmark.

Aircraft flying both at high altitude and at polar latitudes can thus encounter as much as 12 to 20 times the radiation levels found at normal cruising altitudes at lower latitudes [6].

It is thus timely to think about concepts for protective shielding against cosmic radiation in air traffic. Considering that additional weight introduced by protection supplies directly translates into an increase in fuel costs, this is indeed a technically challenging issue. While such a solution is required to be of minimal weight penalty, it has yet to be efficient in shielding highly energetic radiation. In general, the penetrating ability of each type of electromagnetic or particle radiation through matter depends both on its energy as well as on the matter's atomic structure, since these govern the probability for different interaction types to proceed. This implies, for example, that the biological response to ionizing radiation varies with the type of particle as well as its energy and is furthermore specific to cell or tissue type. The so-called effective dose quantifies the radiation hazard by incorporating appropriate weighting factors for each type of radiation as well as for various organs and tissue of the human body [9]. For illustration, we have plotted in Fig. (1) the estimated fraction of the energy-integrated effective dose rate for neutrons, protons and X-ray/Gamma-radiation provided to the total effective dose per flight hour at typical cruising altitudes of about 10 km at the geomagnetic poles and at solar minimum. We have determined the dose rates by folding the corresponding particle fluence spectra [17] with the respective energy dependent effective dose conversion coefficients [9, 18, 19, 20]. One observes that neutrons provide roughly half of the total effective dose rate, while the main contribution comes from high energy neutrons in the MeV to GeV energy range with velocities of up to about 90% of the speed of light. In the next subsection we will hence focus on radiation shielding concepts for high energy neutrons.

1.2 Shielding Concepts for High Energy Neutrons

One possible way of efficiently attenuating highly energetic, very fast neutrons is provided by radiation shielding concepts involving materials, which comprise constituents with comple-

mentary properties in the following sense. The first constituent material contains a large amount of hydrogen and thereby guarantees an efficient slow down and energy loss of very fast neutrons by means of elastic collisions, a process called thermalization. Its efficiency relies on the fact that neutrons have nearly the same mass as hydrogen nuclei (protons) such that in each collision a maximum of their kinetic energy is transferred to the hydrogen nuclei. The second constituent of the shielding solution is characterized by a high ability to absorb slow, thermal neutrons such as boron or compounds thereof. However, as recent experimental data indicate, nanomaterials including boron-containing nanostructures of various dimensions such as nanoparticles, nanotubes or nanoplates enable efficient shielding of thermal neutrons with much less volume and weight compared to purely hydrogen-containing or macroscopic boron particle-containing materials [21]. The data further suggest that the size, conventionally ranging between 1 and 100 billionth of a meter in at least one dimension, as well as the geometry of the nanostructures could have a sizable effect on the shield performance as we have illustrated in Fig. (2).

As concerns the first shielding component required to attenuate highly energetic neutrons in aviation, one natural way would be to use liquid hydrogen (LH_2) as implemented in the so-called cryoplane technology, which we will discuss in some more detail in the next subsection.

1.3 Cryoplane Technology and Tank Layout

LH_2 provides a long-term technological option as alternative fuel, which could reduce the climate impact of air traffic. Compared with conventional kerosene engines, the main benefit of this so-called cryoplane technology is the elimination of both CO_2 and particle emissions, while a lower NO_x emission index is also expected. As a long-term perspective, future hydrogen fuelled electric aircraft may be both CO_2 and NO_x emission free, when equipped with a fuel cell power system [22].

However, challenges for the cyroplane technology emerge from the four times larger storage volume than kerosene for the same energy content and the additional requirement of pressurized storage. For reasons of volume and weight, for aviation, hydrogen as alternative fuel must be cooled down to the liquid state (LH_2, 20 K) and thus necessitates very good insulation of the strorage tanks or pipes. Yet, a large volume of liquid hydrogen within the tanks is beneficial for attenuating highly energetic neutrons, since a large number of hydrogen nuclei (protons) are placed at the disposal for slowing down incident neutrons by elastic collisions. As concerns the incorporation of liquid hydrogen tanks, new aircraft configurations are required. Here, with regards to the increase in energy consumption of LH_2, the optimal tank layout for the aerodynamic efficiency and construction weight has been found to depend on the aircraft category [1].

In the study at hand, it is our aim to evaluate the theoretical potential of the cryoplane technology combined with recent advances in nanoscience to reduce the radiation hazard to humans arising from cosmic radiation at aircraft altitudes. In our analysis, we account for the angular distribution of the atmospheric spectrum of neutrons, which turns out to play a significant role for the identification of tank layouts suitable for radiation protection. For this reason, we will focus on a particular liquid hydrogen tank architecture. It features tanks on top of the fuselage spanning a substantial fraction of the length of the aircraft and bears a large potential for shield weight (and wetted area) trade-offs.

Firstly, we analyse the modifications to the original energy spectrum of cosmic neutrons after propagating through the hydrogen tanks and after being attenuated by elastic collision with hydrogen nuclei. This will on the one hand allow us to determine the fraction of neutrons slowed down to thermal energies before entering the cabin. On the other hand, it motivates the investigation of the shielding effectiveness of novel boron-containing nanomaterials, for example, applied as thin films, foams or pastes at the ceiling of the cabin interior, in relation to the mass penalty. Finally, we will be able to derive

bounds on the achievable reduction in the effective dose within the aircraft cabin.

The paper is organized as follows: after setting the stage for our analysis, in Sec. 2, we determine the net distance a neutron has random-walked after a certain number of elastic collisions with hydrogen nuclei. In Sec. 3, we determine an upper limit on the initial neutron energy, for which the attenuation to thermal energies is guaranteed for realistic tank dimensions. In Sec. 4, we consider the moderating ability of the hydrogen tanks with respect to the high-energy tail of the atmospheric neutron spectrum and derive bounds on the total achievable reduction in the effective dose from neutrons in Sec. 5. Furthermore, in Sec. 6, we provide an estimate of the mass penalty resulting from efficiently shielding the cabin from the thermal neutron flux by means of nanomaterials. Finally, in Sec. 7 we conclude.

2 The Neutron Slow-Down Distance

In reference [20], the angular distribution of cosmic radiation at typical cruising altitudes (10.7 km) has been investigated by means of the Monte Carlo computer code FLUKA. It has been demonstrated that at these altitudes, the assumption of isotropic irradiation is only justified up to some particle-specific maximal energy. Above this energy, anisotropies quickly develop, resulting in a dominant incidence of downward-directed particles, while the particle radiance is exponentially suppressed for increasing solid angle. For neutrons, this transition from isotropic to downward-peaked irradiation starts at roughly 10 MeV.

In the following, it is our aim to estimate the theoretical potential of attenuating cosmic neutrons by means of the cryoplane technology. We therefore consider configurations, which feature LH_2 tanks at the top of the fuselage of the aircraft as depicted in Fig.(3). For the purpose of illustration, we assume the tanks as well as the airframe to be roughly described by cylinders with cross-sectional radii R_t and R_a, and take the tanks to be positioned symmetrically around the vertical axis of the aircraft with a length L_t, which spans

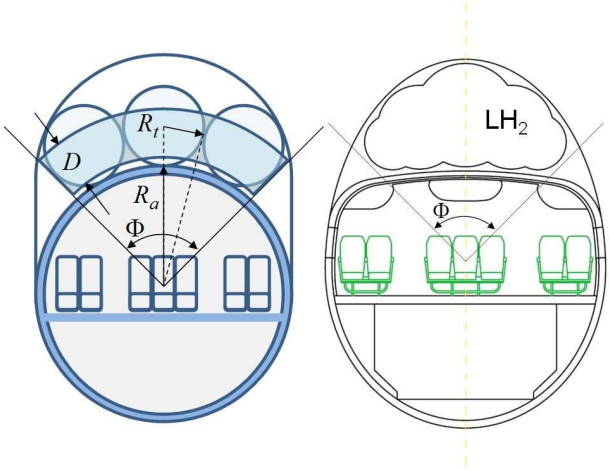

Fig. 3 Left: The cross-sectional view of the cabin with radius R_a and the three LH_2 tanks with radius R_t, and the definition of the angle Φ as well as the characteristic dimension D (see Eq. (1)). Right: An alternative configuration for the storage of LH_2. The figure on the right is adopted from Ref. [3].

a substantial fraction of the aircraft's body. Under these assumptions, from the viewpoint of a passenger seated at the center of the aircraft the fraction F_Ω of the full solid angle $\Omega = 4\pi$ covered by hydrogen tanks is given by,

$$F_\Omega = \frac{\int_\vartheta^{\pi-\vartheta}\int_0^{\Phi}\sin(\theta)\mathrm{d}\theta\mathrm{d}\phi}{4\pi} = \frac{3}{\pi}\frac{\arcsin\left(\frac{1}{1+(R_a/R_t)}\right)}{(1+4(R_a/L_t)^2)^{\frac{1}{2}}}, \qquad (1)$$

where we have used that $\Phi = 6\arcsin(R_t/(R_t + R_a))$ and $\vartheta = \arctan(2R_a/L_t) \ll 1$, while the last inequality assumes $R_a \ll L_t$. One observes that F_Ω and thus the radiation protection of the passenger in the center of the aircraft grows with increasing length L_t and with increasing tank radius R_t for fixed radius of the airframe cross-section R_a. For simplicity, as indicated in Fig. (3), we will in the following take D as the effective thickness of the hydrogen moderator. Let us point out that even if the number or shape of the tanks on top of the fuselage is varied (cf. Fig. (3) on the right for an example), one typically ar-

rives at $0.25 \leq F_\Omega \leq 0.36$ for viable configurations [1, 2, 3, 23].

The next issue we will investigate, is the slow-down distance of fast neutrons impinging on the liquid hydrogen tanks. The achievable efficiency of attenuation depends on how far a neutron with initial energy E_i has random-walked before its energy is moderated to a much smaller energy E_n. This distance, however, varies with the energy of the neutron and decreases with increasing number of experienced elastic collisions, while the neutron traverses the interior of the tanks composed of liquid hydrogen atoms.

Between two collisions, a neutron with energy E_j travels the average distance λ_j, called the mean free path, and is scattered through μ, the average cosine of the scattering angle in the laboratory system. However, λ_j depends on the scattering cross-section σ_s, which describes the probability of a collision to take place and in general, can thus be energy dependent. While it varies rather strongly with neutron energy for $E_i > 0.1$ MeV, only for neutron energies $E_i < 0.1$ MeV, it is a reasonable approximation to assume $\lambda_j = \bar{\lambda} \simeq$ const., since in this case the cross-section is fairly energy independent. Therefore, the general form of the root-mean-square of the average distance squared, $R_{\rm rms} = \sqrt{\langle R^2 \rangle}$ – the net displacement of a neutron after n collisions – depends on the following sum of energy dependent λ_j [24],

$$R_{\rm rms} = \sqrt{2}\left[\sum_{j=1}^{n}\lambda_j^2 + \sum_{j=1}^{n-1}\lambda_j \sum_{k=j+1}^{n}\lambda_k \mu^{k-j}\right]^{\frac{1}{2}}, \tag{2}$$

which only for $\lambda_j = \bar{\lambda} \simeq$ const. reduces to,

$$R_{\rm rms} = \left[\frac{2n}{1-\mu}\right]^{\frac{1}{2}}\bar{\lambda}, \tag{3}$$

where $\mu = 2/3A$ in the laboratory system, with A denoting the atomic mass and $A = 1$ as well as $\mu = 2/3$ for hydrogen. Here, the number n of elastic collisions governs the energy loss of a neutron from an initial energy E_i to an energy E_n, which on average, is determined by,

$$\begin{aligned} n &= \frac{1}{\xi}\ln\left(\frac{E_i}{E_n}\right), \text{ with} \\ \xi &= 1 - \frac{(A-1)^2}{2A}\ln\left(\frac{A+1}{A-1}\right), \end{aligned} \tag{4}$$

where ξ, the mean energy loss per collision, is fixed by the atomic weight A of the scattering nuclei. One observes that since $A = 1$ for hydrogen, the average energy loss per collision is maximized with $\xi = 1$ in comparison to other nuclei with $A > 1$ and $\xi < 1$. For example, an average number of 18 collisions suffices to thermalize a neutron with $E_i = 2$ MeV that is to reduce its energy by roughly 8 orders of magnitude to the thermal energy $E_n = 0.025$ eV.

It should be noted that in reality, both the free path lengths and scattering angles will cover a broad distribution, while Eqs. (2)–(4) refer to resulting average values. This implies that even if the neutron traverses a moderating medium, which has an extension smaller than the total average mean free path λ, the probability that it underwent one or even more interactions with hydrogen nuclei (protons), does not vanish. This is captured in the exponential relation describing the drop in intensity I_0 of a parallel neutron beam of a given energy E to an intensity $I(x)$ after passing through a sample of thickness x,

$$\begin{aligned} I(E,x) &= I_0(E)e^{-\frac{x}{\lambda(E)}}, \text{ with} \\ \lambda(E) &= \frac{1}{N\sigma(E)}, \end{aligned} \tag{5}$$

where N denotes the atom density, which is $N = 4.23 \cdot 10^{22}\,\mathrm{cm}^{-3}$ for liquid hydrogen at 20 K, and σ is the total cross-section. One observes that in order for most neutrons of a given energy to unimpededly propagate through the moderator such that $I(x)/I_0 \simeq 1$, the thickness x is required to be significantly smaller than the total mean free path $x \ll \lambda$.

In general, Eq. (5) implies that while the neutrons traverse the hydrogen tanks, their energy spectrum will be modified in an intricate way. In order to derive a first estimate of the attenuation

efficiency of the liquid hydrogen tanks with regards to cosmic neutrons, we will therefore take the following simplifying approach. We will in a first step determine the average slow-down distance $R_{\rm rms}(E_i)$ required according to Eq. (2) for neutron thermalization as a function of the initial neutron energy E_i. In a second step, we will compare this distance with the extension D, assuming realistic ranges for the geometrical parameters describing the tank architecture and the aircraft. We will then be able to consider two limiting cases, the first one resulting for initial neutron energies E_i, for which $R_{\rm rms}(E_i) \lesssim D$. In this case, a substantial slow-down of the impinging neutrons will be achieved by the moderator down to thermal energies. For the second case, $R_{\rm rms}(E_i) > D$, as discussed before, Eq. (5) then implies that a small fraction of neutrons $1 - e^{-D/\lambda}$ will have had at least one interaction, when traversing through the moderator. We will derive both an upper and a lower bound on the resulting reduction in the effective dose rate and thereby demonstrate that the result is fairly insensitive to the number of collisions assumed here. This approach will thus allow us to estimate the attenuation efficiency of the hydrogen filled tanks for all neutron energies of the atmospheric spectrum, up to the very highest initial energies.

3 Neutron Thermalization by Liquid Hydrogen

In general, the requirement that an impinging neutron with energy E_i is thermalized – that is attenuated to thermal energies, while traversing the moderator – can be determined from Eq. (4) and translates into the following condition on the required average number of collisions,

$$n_t = 17.50 + \ln\left(\frac{E_i}{\rm MeV}\right), \qquad (6)$$

where we have used that $A = \xi = 1$ for hydrogen as well as inserted $E_n = 0.025$ eV for the energy of the thermalized neutron. In Fig. (4), we have plotted the average distance $R_{\rm rms,t}$ resulting from $n = n_t$, which is required for thermalizing a neutron with initial energy E_i. For comparison,

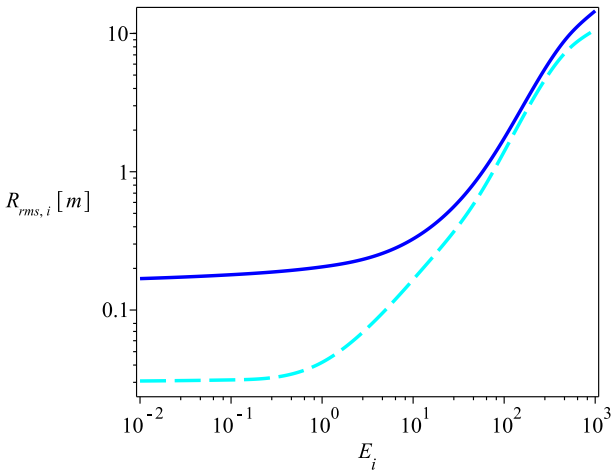

Fig. 4 The average distance a neutron random-walks within a liquid hydrogen moderator after one collision, $R_{\rm rms,1}$, (dashed line) and after n_t collisions, $R_{\rm rms,t}$, when it is thermalized (solid line) as a function of its initial energy E_i.

we have also displayed the average net displacement $R_{\rm rms,1}$ of the neutron after being scattered the first time. Interestingly, for high initial neutron energies E_i, the average displacement $R_{\rm rms,t}$ of a neutron after $n = n_t$ collisions for thermalization is of the same order of magnitude as the average displacement $R_{\rm rms,1}$ after the first scattering event. The reason is that, as mentioned before, the elastic neutron-proton scattering cross-section exhibits a strong energy dependence between 0.1 MeV and 1 GeV, decreasing by 3 orders of magnitude, while it is fairly constant for energies below 0.1 MeV with a slight rise at thermal energies [26]. Accordingly, at high neutron energies, already after the first collision, the mean free path is greatly reduced such that the sum in Eq. (2) defining $R_{\rm rms,t}$ fairly quickly converges to its final value (after n_t collisions). This is opposed to the thermalization process of neutrons with energies < 0.1 MeV, because in this case, the mean free path is fairly independent of energy leading to equally large contributions $\bar{\lambda}$ after each collision as described by Eq. (3).

Let us recall that the atmospheric neutron flux at aircraft altitudes can be taken to be isotropic for energies < 10 MeV. According to Fig. (4), this implies that neutrons of the isotropic part

of the spectrum are thermalized after passing through an average moderator thickness of 30 cm. In this case, a passenger in the center of the aircraft is subject to a thermal neutron radiance in a fraction F_Ω of the solid angle (see Eq. (1)), while being still affected by the unattenuated neutron radiance incident from solid angles not covered by the hydrogen tanks. As mentioned in the introduction and as we will demonstrate in Sec. 6, the thermal neutron flux can be efficiently absorbed by the help of thin layers of boron containing nanomaterials, for example, applied at the ceiling of the aircraft cabin.

Consequently, we are now in a position to determine the achievable reduction in the effective dose rate for a moderator thickness $D > 30$ cm and for neutrons with $E_i \leq 10$ MeV. For this purpose, we take the particle fluence rate (corresponding to the particle radiance integrated over the full solid angle) multiplied by F_Ω and folded with the appropriate energy dependent conversion coefficients between neutron fluence rate and effective dose rate. Since typically, $0.25 \leq F_\Omega \leq 0.36$, we arrive at a reduction in the effective dose rate between 25% and 36% for the passenger seated in the center of the aircraft, with respect to all neutrons of the atmospheric spectrum with $E_i \leq 10$ MeV. Let us note again that this result holds as long as the thickness of the hydrogen moderator is larger than 30 cm.

As mentioned before, around energies $E_i \gtrsim 10$ MeV, anisotropies in the neutron radiance quickly develop, which leads to a strong dominance of downward-directed neutrons. It is therefore justified to assume that the great majority of these highly energetic neutrons need to pass through the hydrogen tanks, before having a chance of hitting a passenger seated at the center of the aircraft. As long as $D \gtrsim R_{\mathrm{rms,t}}(E_i)$, on average, the attenuation efficiency still suffices to thermalize all neutrons before they leave the moderator and enter the cabin of the aircraft. For example, assuming a moderator thicknesses of 1.50 m as well as $F_\Omega = 0.36$, the majority of neutrons of the spectrum with initial energies $10\,\mathrm{MeV} \leq E_i \leq 87\,\mathrm{MeV}$ would be downward-directed, pass through the hydrogen tanks, and become thermalized.

4 High-Energy Neutron Attenuation

In this section, we estimate the achievable reduction of the effective dose rate resulting from neutrons with initial energies E_i, for which the extension D of the moderator is smaller than the mean free path, $D < R_{\mathrm{rms,t}}(E_i)$. As mentioned before, for $D > 30$ cm this corresponds to $E_i > 10$ MeV such that we can in the following take these highly energetic neutrons to be dominantly downward-directed. With respect to the passenger in the center of the aircraft, this means that while the attenuation efficiency of the hydrogen moderator decreases according to Eq. (5), practically *all* neutrons of the atmospheric spectrum with energies above $E_i > 10$ MeV pass through the hydrogen tanks. As discussed before, Eq. (5) then implies that a small fraction of neutrons $1 - e^{-D/\lambda}$ will have *at least one* interaction, when traversing through the moderator. As a first step, in order to gain a conservative lower bound on the reduction of the resulting neutron effective dose equivalent, we will thus assume that the fraction of neutrons $1 - e^{-D/\lambda(E)}$ will have *one* interaction, when traversing through the moderator, while we neglect the fraction of neutrons with *more than one* interaction. In a second step, we derive an upper bound on the achievable reduction in the effective dose equivalent, by assuming that the number of interactions of the fraction of neutrons $1 - e^{-D/\lambda(E)}$ was sufficient for thermalization. Note that interestingly, as discussed in Sec. 3, the average displacement $R_{\mathrm{rms,t}}$ of a neutron after $n = n_t$ collisions for thermalization is of the same order of magnitude as the average displacement $R_{\mathrm{rms,1}}$ after the first scattering event at large neutron energies > 0.1 MeV.

Our results for the effective dose equivalent per energy interval are depicted in Fig. (5) and demonstrate that between 87 and several hundred MeV a non-negligible reduction in the effective dose equivalent per energy and time interval can be achieved. One also observes that the dependence on the assumed number of collisions is rather weak. In the next section, we present our

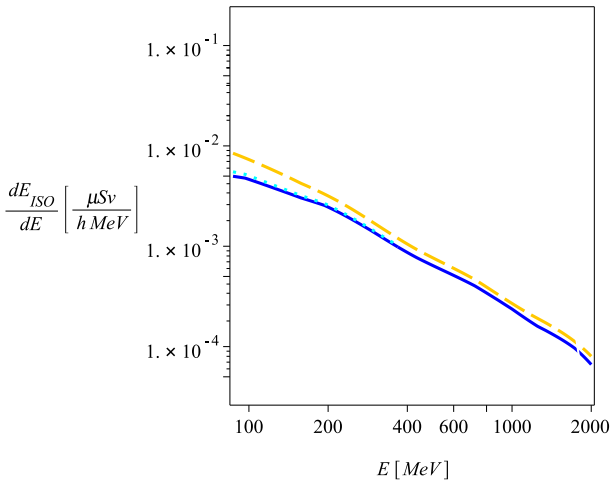

Fig. 5 Effective dose rate per energy interval in units of micro-Sievert (μSv) per hour per MeV as a function of the neutron energy E for the atmospheric spectrum (dashed) as well as the lower (solid) and upper (dotted) limit for the neutrons, which have passed through the liquid hydrogen moderator with an average extension of $D = 1.5$ m.

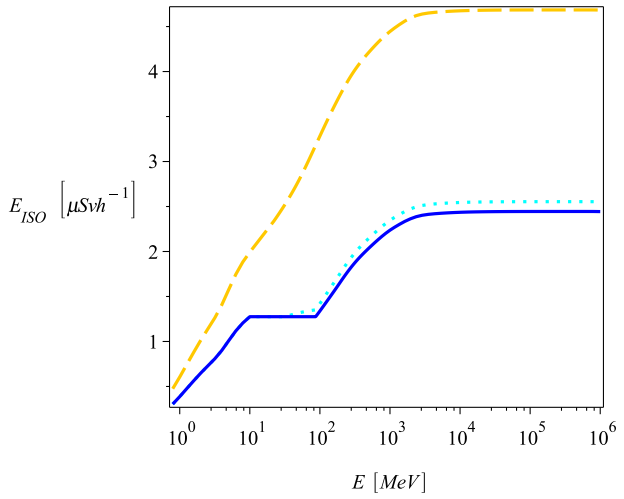

Fig. 6 Effective dose rate for neutrons up to an energy E_i in micro-Sievert (μSv) per hour for the atmospheric spectrum (dashed) as well as the corresponding lower (solid) and upper (dotted) limit at the center of the cryoplane assuming an average depth of filling of the hydrogen tanks of $D = 1.5$ m.

results for the achievable total neutron effective dose reduction at the center of the cryoplane considering the full range of neutron energy in the atmospheric spectrum.

5 Reduction in the Effective Dose Rate

In Fig. (6), we compare the effective dose rate E_{ISO} resulting from all neutrons of the atmospheric spectrum up to an energy E_i with the corresponding upper and lower bounds in the aircraft cabin derived for the considered cryoplane configuration with $F_\Omega = 0.36$ and an average depth of filling of the hydrogen tanks of $D = 1.5$ m. For energies $E_i < 10$ MeV, one observes that since the neutron radiance is isotropic, only the fraction F_Ω actually passing through the hydrogen tanks is thermalized and shielded before entering the cabin such that the effective dose rate still grows in proportion to the corresponding dose value of the atmospheric spectrum. For $10\,\mathrm{MeV} < E_i < 87\,\mathrm{MeV}$, the majority of neutrons is downward-directed and can be attenuated to thermal energies, since $D > R_{\mathrm{rms,t}}(E_i)$ (cf. the discussion in Sec. 3). Accordingly, in this energy range, neutron moderation is most efficient: one observes that E_{ISO} only slightly grows in the case of the upper bound derived in the last section, while being constant in the case of the lower bound. The reason is that in the first case, we assumed neutrons with energies $E_i > 87$ MeV to have at most *one* elastic collision within the tank such that a few highly energetic neutrons are down-scattered to energies > 32 MeV according to Eq. (4) for $n = A = \xi = 1$. In the second case, we assumed the same fraction of neutrons to have been thermalized. In conclusion, one arrives at an impressive reduction of the total neutron effective dose rate in the center of the aircraft between 45% and 48% compared with its value in the free atmosphere.

6 Absorption of Thermal Neutrons

This section aims at estimating the mass penalty resulting from introducing a second shielding component to absorb the thermal neutron flux, which is generated by the attenuation of high energy neutrons within the hydrogen tanks. This

could, for example, efficiently be realised, by applying a thin layer of a boron-containing nanocomposite in the form of a film, paste or foam at the ceiling of the aircraft cabin. For this purpose, let us recall that the mass attenuation coefficient χ discussed in the introduction is a metric for the shielding performance in relation to the mass penalty. Together with the density ρ of the neutron absorbing material, it therefore determines the material thickness required to shield a certain fraction of an incoming neutron beam with initial intensity I_0. The half- $x_{1/2}$ and tenth-thickness $x_{1/10}$, which refer to the material thickness required to absorb 50% and 90% of the thermal neutron flux such that the transmitted flux respectively is $I(x_{1/2}) = 1/2\,I_0$ and $I(x_{1/10}) = 1/10\,I_0$, are given by,

$$x_{1/2} = \frac{\ln(2)}{\chi\rho} \tag{7}$$

$$x_{1/10} = \frac{\ln(10)}{\chi\rho} \simeq 3.32\,x_{1/2}, \tag{8}$$

where ρ is the density of the nanocomposite layer. Approximating the geometry of the aircraft cabin again by a hollow cylinder, we can then estimate the respective mass penalties $\Delta M_{1/2}$ and $\Delta M_{1/10}$ resulting from coating a fraction F_ϕ of the lateral area at the ceiling of the aircraft with a nanocomposite layer of thickness $x_{1/2}$ and $x_{1/10}$,

$$\Delta M_{1/2} = F_\phi\,\rho A x_{1/2} \simeq \ln(2)\,\frac{F_\phi A}{\chi} \tag{9}$$

$$\Delta M_{1/10} \simeq 3.32\,\Delta M_{1/2}, \text{ with} \tag{10}$$

$$A = 2\pi R_a L_t, \tag{11}$$

where $F_\phi = \Phi/2\pi = 3\arcsin(R_t/(R_t+R_a))/\pi$ in correspondance to the fraction of the solid angle covered by the hydrogen tanks in Eq. (1). For example, for $R_a = 1.9$ m, $R_t = 1$ m and $L_t = 25.0$ m, $F_\phi = 0.3$ and $\chi = 1.7\,\mathrm{cm}^2/\mathrm{g}$ for boron-nitride nanotube (BNNT)/polyimide nanocomposites with 5% BNNTs (cf. Fig. (2)), this would result in $x_{1/2} = 3.1$ mm and $x_{1/10} = 1.03$ cm and mass penalties of $\Delta M_{1/2} = 407.2$ kg and $\Delta M_{1/10} = 1352.1$ kg. $\Delta M_{1/2}$ seems to be an acceptable mass penalty, which presumably would result in an increase of mission fuel below 0.5% even for a short- to medium range aircraft, while at the same time yielding an efficient reduction of the thermal neutron fluence by 50%. For achieving a further reduction of the thermal neutron intensity to $10\%I_0$, the associated mass penalty $\Delta M_{1/10}$ does not seem justifiable. Note, however, that besides a high neutron shielding efficiency, boron-nitride nanotubes embedded in a polymer matrix have been found to exhibit extremely high strength, optical transparency and UV shielding ability at minimal weight penalty [21]. In principle, this would allow for multifunctional applications of boron-nitride nanotube containing nanocomposites besides radiation protection including use for structural integrity and thus indirectly reduce the associated mass penalty.

7 Conclusions

In the study at hand we confronted future trends in air travel such as increased polar route frequencies and cruising altitudes with the associated risk arising from cosmic radiation. We identified and evaluated a radiation shielding concept based on the cryoplane technology and recent advances in nanoscience. As a key result, we demonstrated that as a surplus to its beneficial impact on the climate, liquid hydrogen as future option for aircraft fuel bears a significant potential for cosmic radiation protection. To this end, we analysed the cosmic radiation fields at aircraft altitudes, demonstrating that in air traffic the dominant hazard to humans arises from highly energetic cosmic neutrons. We considered a tank layout, where the tanks are positioned on top of the fuselage extending over a substantial fraction of its longitudinal extension. For a passenger in the center of the aircraft, this architecture was found to be beneficial even for attenuating highly energetic neutrons with energies above 10 MeV. Since these neutrons are mainly downward-directed, most of them pass through the tanks before entering the cabin. In contrast, at lower energies, the neutron radiance is fairly isotropic such that a smaller fraction of the fluence passes through the tanks before penetrat-

ing the interior of the aircraft cabin. Still, a trade-off exists between the anisotropic fluence and the significantly reduced mean free path between elastic collisions at lower neutron energies. More, precisely, the average net displacement a neutron travels within a liquid hydrogen moderator until it is thermalized – decreases with neutron energy. For realistic geometrical parameters, on average, the extension of the tank was found to be sufficient to slow-down and thermalize all neutrons incident on the tank with original energies below roughly $50-90$ MeV.

We verified that for example, thin films, foams or pastes of boron-containing nanocomposites applied to the ceiling of the cabin could effectively absorb these thermal neutrons at minimal weight penalty. Thus, we demonstrated that by combining a hydrogenous neutron moderating medium with a boron-containing strongly absorbing material a considerable fraction of neutrons could be completely removed from the spectrum within the cabin interior. Finally, we derived both a lower and an upper bound on the achievable reduction of the effective dose rate E_{ISO} for neutrons. Considering a passenger seated in the center of the aircraft and an average moderator thickness of $D = 1.5$ m, we for example, arrived at a reduction of the neutron induced E_{ISO} between 45% and 48%.

Let us in the following summarize a few key facts relevant for the interpretation of this result. First of all, while neutrons provide with roughly 50% the dominant contribution to the total effective dose in the cabin, the presence of the liquid hydrogen filled tanks is expected to further reduce the effective dose induced by cosmic protons, which account with roughly 40% for the second largest contribution. It should further be noted that the stated decrement in the neutron effective dose is merely due to the presence of the hydrogen tanks and the boron-containing nanomaterial applied to the ceiling and does not include the effects of further scattering processes within the cabin. The latter, however, provide a sizable, position dependent additional total dose reduction of up to 25%, arising from particle interactions with other hydrogenous material, for example, polymeric material such as cellulose containing baggage or cargo, as well as humans within the fuselage. While this effect is present in any aircraft configuration, the cryogenic technology offers considerable advantages in radiation protection over a kerosene fuelled aircraft: the volume of liquid hydrogen is four times larger at the same energy content as kerosene, the hydrogen content is 33% larger than of hydrocarbon fuel like kerosene and the tank layout on top of the fuselage allows to attenuate downward-directed, highly-energetic neutrons. Clearly, the effective dose rate will vary with the passenger seat position, increasing towards the windows, and furthermore will grow with hydrogen fuel consumption. Yet, in summary, we can infer that combined with nanotechnology, the cryogenic technology bears a significant potential for economic radiation protection in air traffic, while at the same time allowing a sustainable growth of aviation with an extremely low impact on the environment.

References

[1] *Final Technical Report 2003*. Project: GRD1-1999-10014 European Commision, 5th Framework, 2003.

[2] Westenberger, A., Airbus Germany GmbH, *Presentation at EHEC-Conference*. Grenoble, France, 2003.

[3] Donus, F., Kirchner, D., Myrczik, M., Schubert, H., Schwarze, M., Group 7, *Aircraft design seminar*. IFB, University of Stuttgart, 2007.

[4] Ponater, M. et al., *Proceedings of the AAC-Conference*. Friedrichshafen, Germany, 2003.

[5] Holmes-Siedle, A., Adams, L., *Handbook of radiation effects*. Oxford, 2002.

[6] Newcome, L. R., *Aeronaut. J.*, Vol. 110, No. 1111, pp. 623-626, 2006.

[7] Bentley, R. D. et al., *Proceedings of the Second Solar Cycle and Space Weather Euroconference*. 2002.

[8] Pukkala, E. et al., *Av. Space. Env. Med.*, Vol. 74, No.7, 2003.

[9] International Commission on Radiological Pro-

tection, *ICRP Publication 60*. Pergamon Press, Oxford, 1991.

[10] Dyer, C. et al., *Proceedings of the ICAS Congress 2000*. Harrogate, UK, 6.4.4, 2000.

[11] Chulliat, A. et al., *J. Geophys. Res.*, 115, B07101, 2010.

[12] United Airlines, *Polar Operations 1996-2010, briefing to Cross-Polar Working Group*. Paris, 2010.

[13] IATA, *IATA Economics 2011*. 2011.

[14] Mertens, C. J. et al., *Proceedings of the 1st AIAA Atmospheric and Space Environments Conference 2009*. San Antonio, Texas, p. 3633, 2009.

[15] Li, S. W. et al., *J. Environ. Rad.*, Vol. 94, Iss. 2, pp. 98-106, 2007.

[16] Bartlett, D.T. et al., *Radiat. Prot. Dosimetry*. Vol. 91, Iss. 4, pp. 365-376, 2000.

[17] Roesler, S. et al., *Radiat. Prot. Dosimetry*. Vol. 98, Iss. 4, pp. 367-88, 2002.

[18] Sato, T. et al., *Phys. Med. Biol.*, 54, p. 1997, 2009.

[19] Ferrari, A., Pelliccioni, M. and Villari, R., *Radiat. Prot. Dosimetry*. 108, Iss. 2, pp. 91-105, 2004.

[20] Battistoni, G., Ferrari, A., Pelliccioni, M. and Villari, R., *Radiat. Prot. Dosimetry*. 112, Iss. 3, pp. 331-343, 2004.

[21] NASA, *The Technology Gateway*. TOA 107. NP-2011-03-359-LaRC, LAR-17535-1, LAR-17668-1, LAR-17780-1, LAR-17902-1,. LAR-17991-1, and JLab 1265 2011.

[22] Kuhn, H. et al., *CEAS Conference*. Venice, 2011.

[23] Schwarze, M., Technical University of Munich, *Private communication*. 2012.

[24] Nellis, W. J., *AJP*. 45, Iss. 5, pp. 443, 1977.

[25] Stacey, W. M., *Nuclear reactor physics*. Wiley-VCH, 2007.

[26] Nakamura, K. et al. (Particle Data Group). *J. Phys.*, G37, 075021, pp. 331-343, 2010.

7.1 Copyright Statement